nature structural & molecular biology

The ABC-F protein EttA gates ribosome entry into the translation elongation cycle

Grégory Boël[1,2], Paul C Smith[1,8], Wei Ning[3], Michael T Englander[3,4,8], Bo Chen[1], Yaser Hashem[5,6], Anthony J Testa[1], Jeffrey J Fischer[7,8], Hans-Joachim Wieden[7], Joachim Frank[1,5,6], Ruben L Gonzalez Jr[3] & John F Hunt[1,2]

ABC-F proteins have evaded functional characterization even though they compose one of the most widely distributed branches of the ATP-binding cassette (ABC) superfamily. Herein, we demonstrate that YjjK, the most prevalent eubacterial ABC-F protein, gates ribosome entry into the translation elongation cycle through a nucleotide-dependent interaction sensitive to ATP/ADP ratio. Accordingly, we rename this protein energy-dependent translational throttle A (EttA). We determined the crystal structure of *Escherichia coli* EttA and used it to design mutants for biochemical studies including enzymological assays of the initial steps of protein synthesis. These studies suggest that EttA may regulate protein synthesis in energy-depleted cells, which have a low ATP/ADP ratio. Consistently with this inference, EttA-deleted cells exhibit a severe fitness defect in long-term stationary phase. These studies demonstrate that an ABC-F protein regulates protein synthesis via a new mechanism sensitive to cellular energy status.

Most genomes encode multiple ABC superfamily[1] proteins. These proteins are named after their stereotypical ABCs, which share characteristic sequence motifs involved in ATP hydrolysis. The Walker A and B motifs participate in binding and hydrolyzing the β and γ phosphates of ATP and are shared with a larger group of mechanically active enzymes that includes the F1 and AAA+ ATPases and the superfamily I and superfamily II helicases[2]. However, the C motif or signature sequence, with consensus LSGGQ, is found exclusively in ABC ATPases[1]. These residues drive a mechanical power stroke involving formation of an 'ATP-sandwich dimer'[3–5] in which the LSGGQ from one subunit reciprocally encapsulates the ribose and triphosphate of an ATP molecule bound to the Walker motifs in the other subunit.

Although transporters in the ABC superfamily (ABC transporters) represent the most common molecular architecture used to couple transmembrane transport to ATP hydrolysis[6], the superfamily also includes soluble proteins performing diverse biochemical functions. These include UvrA[7] and Rad50 (ref. 8), which function in DNA repair, and also eEF3 (ref. 9) and ABCE1 (RLI1)[10–13], which are translation factors. ABCE1 binds to the ribosomal aminoacyl-tRNA–binding (A) site in eukaryotic and archaeal post-termination complexes to assist ribosome recycling. The eEF3 protein has been proposed to stimulate the release of deacylated tRNAs from the tRNA-exit (E) site of ribosomes[14,15] and, more recently, to assist recycling of yeast post-termination ribosomal complexes[16]. ABC-F[17,18] and RbbA[19,20] proteins also interact with ribosomes, but their exact biochemical functions remain uncharacterized.

ABC-F proteins (ABC-Fs) compose the most pervasively distributed soluble-protein family within the ABC superfamily. Multiple ABC-F family members are encoded in all eukaryotic and most eubacterial genomes[21], including three in humans, two in *Saccharomyces cerevisiae*, five in *Arabidopsis thaliana* and four in *E. coli* (**Fig. 1** and **Supplementary Fig. 1**). ABC-Fs have two tandem ABCs separated by an ~80-residue linker in a single polypeptide chain. Pfam[22] identifies this linker as a conserved domain (PF12848 or ABC_tran_2) distinct from the ATPase domains (PF00005 or ABC_tran). PF12848 is found in other proteins with diverse organizations generally including at least one ABC domain. However, it is not found in ABC-E or eEF3, which instead contain different domains[12,15] not found in ABC-Fs. Moreover, although ABC-Fs show stronger sequence similarity to eEF3 than to other soluble ABC proteins (**Fig. 1** and **Supplementary Fig. 1**), eEF3 is more closely related to several ABC transporters than to ABC-Fs. Therefore, ABC-Fs represent a distinct phylogenetic lineage that probably evolved independently from the other soluble ABC protein families, and they probably have a different biochemical function.

Despite their ubiquitous distribution, no ABC-F protein has had its exact function elucidated, although some seem to have a role in protein synthesis. The N-terminal domain of GCN20, a yeast ABC-F, modulates a ribosome-associated kinase that regulates translation upon amino acid starvation[23,24]. However, this domain is not found in

[1]Department of Biological Sciences, Columbia University, New York, New York, USA. [2]Northeast Structural Genomics Consortium, Columbia University, New York, New York, USA. [3]Department of Chemistry, Columbia University, New York, New York, USA. [4]Integrated Program in Cellular, Molecular and Biomedical Studies, Columbia University, Medical Center, New York, New York, USA. [5]Department of Biochemistry, Columbia University Medical Center, New York, New York, USA. [6]Howard Hughes Medical Institute, Columbia University Medical Center, New York, New York, USA. [7]Department of Chemistry and Biochemistry, University of Lethbridge, Lethbridge, Alberta, Canada. [8]Present addresses: Department of Molecular Biology, Memorial Sloan-Kettering Cancer Center, New York, New York, USA (P.C.S.), Department Biochemistry and Biophysics, University of Pennsylvania, Philadelphia, Pennsylvania, USA (M.T.E.) and Department of Biological Sciences, University of Calgary, Calgary, Alberta, Canada (J.J.F.). Correspondence should be addressed to J.F.H. (jfhunt@biology.columbia.edu) or R.L.G. (rlg2118@columbia.edu).

Received 13 May 2013; accepted 21 November 2013; published online 5 January 2014; doi:10.1038/nsmb.2740

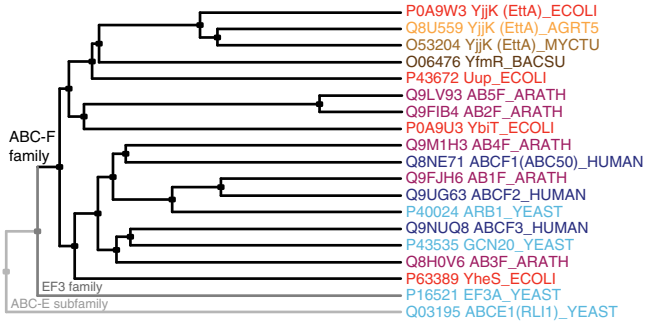

Figure 1 ABC-F phylogeny. Cladogram produced with CLUSTAL-Ω and labeled with Swiss-Prot species codes, showing two bacterial orthologs of EttA (from *Agrobacterium tumefaciens* and *Mycobacterium tuberculosis*), one bacterial paralog of EttA (YfmR from *Bacillus subtilis*), two non–ABC-F family proteins containing tandem ABC domains (eEF3 and ABCE1 from *S. cerevisiae*) and all ABC-F proteins from *E. coli* (red), *S. cerevisiae* (cyan), *A. thaliana* (purple) and *Homo sapiens* (blue). All of these ABC-F proteins, but neither eEF3 nor ABCE1, contain the PF12848 domain in addition to tandem ABC domains.

other ABC-F families, and the established activity of GCN20 does not require its ABC domains. ARB1, the second yeast ABC-F, is essential and impairs ribosome biogenesis upon depletion[25]. Human ABC50 (ABC-F1) influences translation initiation at an internal ribosome entry site (IRES) *in vitro*; consistently with a broader role in translation initiation, a hydrolysis-deficient mutant of ABC50 causes polysome depletion *in vivo*[18]. In contrast, the *E. coli* ABC-F protein Uup has been proposed to function in DNA recombination[26,27]. Nothing is known about the functions of the other *E. coli* ABC-Fs[28], which were given the provisional names YbiT, YheS and YjjK during annotation of the *E. coli* K12 genome (**Fig. 1** and **Supplementary Fig. 1**).

We set out to elucidate the biochemical and physiological functions of *E. coli* YjjK, using a combination of structural, enzymological and genetic methods. This protein has orthologs in more than half of eubacteria, making it the most widespread of the >20 phylogenetically distinct ABC-F classes in eubacteria. We propose renaming this protein energy-dependent translational throttle A (EttA) on the basis of our results presented below, which demonstrate that it is a translation factor that gates ribosome entry into the translation elongation cycle through a nucleotide-dependent interaction sensitive to ATP/ADP ratio.

Crystal structure of *E. coli* EttA

We solved the X-ray crystal structure of *E. coli* EttA by using single-wavelength anomalous diffraction from selenomethionine-labeled protein. This nucleotide-free structure, to our knowledge the first determined for any ABC-F protein, was refined at 2.4-Å resolution to an R_{free} factor of 18.3% (**Table 1**, **Fig. 2a**,**b** and **Supplementary Figs. 1–4**). The asymmetric unit contains a domain-swapped dimer with only minor deviations from two-fold symmetry (**Fig. 2a**). Purified EttA participates in a slowly reversible monomer-dimer equilibrium (**Supplementary Fig. 5a**) that favors the monomer at the ~7-μM to 20-μM concentration measured *in vivo*[29] but the dimer at the ~240-μM concentration used for crystallization. *In vitro* translation assays presented below suggest that the monomer form of EttA regulates protein synthesis because it is active at a 3-μM concentration at which the monomer predominates in solution (**Supplementary Fig. 5a**). This inference is confirmed by the results in ref. 30, which reports the cryo-EM structure of a functional complex of EttA with 70S ribosomes that was generated with equivalent *in vitro* translation reactions. In the domain-swapped dimer of EttA (**Fig. 2a**), ABC1 from one protomer interacts with ABC2 from the other protomer. The cryo-EM structure of EttA[30] indicates that this ABC1–ABC2 complex (**Fig. 2b**), composing half of the dimer structure, represents the active form of EttA.

The tandem ABC domains in EttA are canonical in structure except for one insertion of substantial size in each domain (**Fig. 2a**,**b** and **Supplementary Figs. 1** and **2**). These insertions, dubbed the 'arm' in ABC1 and the 'toe' in ABC2, occur in the loop after the first of the three α-helices in the ABCα subdomain, which is the primary site of transmembrane-domain contact in ABC transporters. The arm is a 45-residue α-helical hairpin spanning amino acids 95–139, whereas the toe is a 12-residue antiparallel β-hairpin spanning amino acids 414–423. We hypothesized, on the basis of their structural uniqueness and location, that these structures mediate important functional interactions, an inference verified below for the arm.

We observed in the crystal structure of EttA minor structural variations at two other sites in the ABC domains: at the C terminus of the ABCβ subdomain and in the segment preceding the LSGGQ motif, both of which are frequent sites of structural diversity in ABC proteins[31]. The catalytic motifs in EttA are canonical, with two exceptions. The first is the lack of an aromatic residue in most EttA orthologs at the C terminus of the first β-strand in the ABCβ subdomain of ABC1, at a position where an aromatic residue typically stacks with the A base of ATP (**Supplementary Fig. 1**). The second is the substitution of glutamate for glutamine in the LSGGQ motifs in ABC1 of all orthologs and in ABC2 of most orthologs (i.e., making their sequences LSGGE). We found less conservative substitutions at this site in ABC1 in some other ABC-F family members

Table 1 Data collection and refinement statistics[a]

	YjjK (EttA)
Data collection	
Space group	$P2_1$
Cell dimensions	
a, *b*, *c* (Å)	45.4, 233.5, 54.1
α, β, γ (°)	90.0, 91.3, 90.0
Resolution (Å)	50.0–2.4 (2.44–2.40)
R_{sym}	14.3% (57.7%)
$I / \sigma I$	14.1 (2.0)
Completeness (%)	93.7% (83.2%) for $I > -\sigma I$
Redundancy	6.5 (3.2)
Refinement	
Resolution (Å)	50.0–2.40 (2.46–2.40)
No. reflections	41,106 (2,328)
R_{work} / R_{free}	18.3% (24.0%) / 24.3% (32.0%)
No. atoms	8,904
Protein	8,376 (23 alternate conformations)
Ligand/ion	132
Water	396
B factors (Å^2)	
Protein	35.3
Ligand/ion	50.7
Water	31.7
r.m.s. deviations	
Bond lengths (Å)	0.006
Bond angles (°)	1.23

[a]Data collection statistics correspond to a data set derived from a single crystal. Values in parentheses are for the highest-resolution shell. Data collection statistics come from SCALEPACK, and other statistics come from PHENIX.

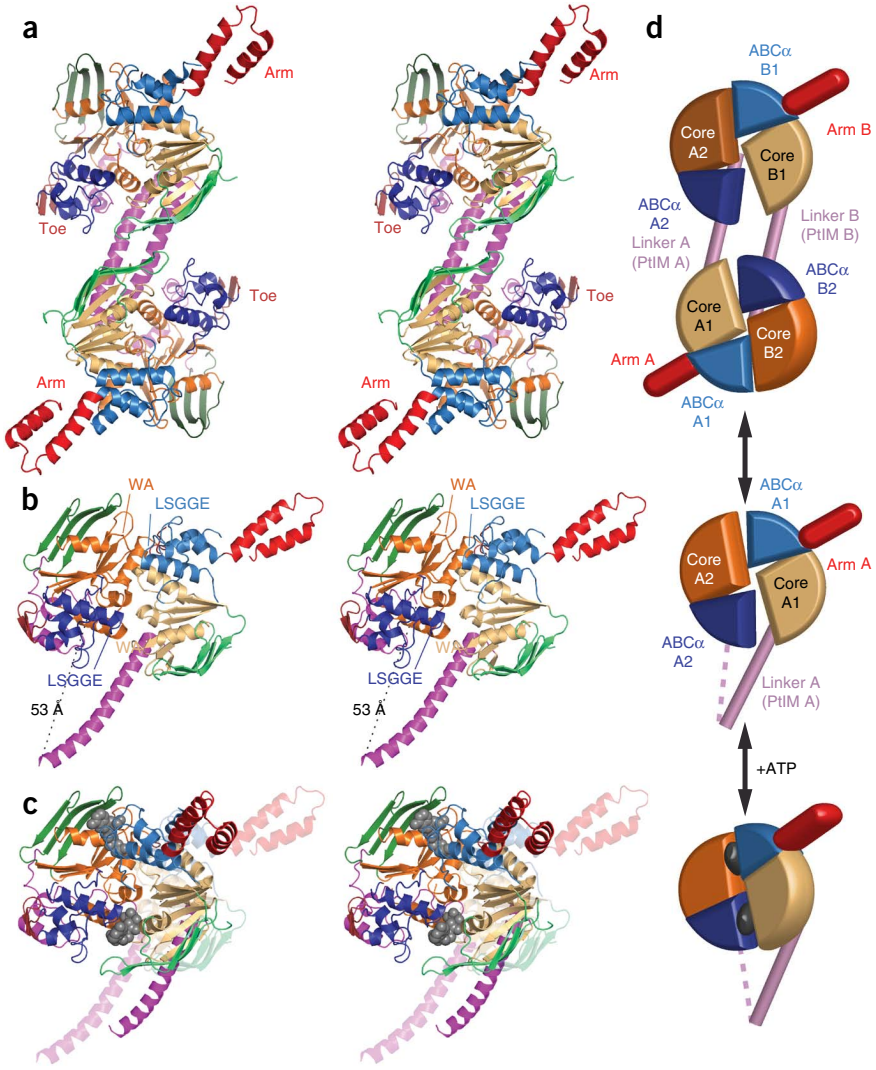

Figure 2 Crystal structure of *E. coli* EttA. (**a**) Stereopair showing the nucleotide-free EttA dimer in the asymmetric unit (**Table 1**). The ABC domains in each protomer are colored lighter (ABC1) and darker (ABC2) shades of similar colors (green, ABCβ; tan-orange, F1-like core; blue, ABCα subdomains; red, arm and toe motifs; magenta, PtIM[30]). (**b**) Equivalently colored stereopair showing a magnified view of one interacting ABC1–ABC2 domain pair in the EttA dimer (generated by deletion of residues 1–286 in protomer A and 278–555 in protomer B), which provides a model for the nucleotide-free conformation of the EttA monomer. Labels indicate the Walker A (WA) motif in the FI-like core and the LSGGE signature sequence in the ABCα subdomain. The Walker B motif (Φ_4DE, with Φ being any hydrophobe and terminating in catalytic base) is located between the WA and LSGGE motifs within each ABC. (**c**) Stereopair showing models for the nucleotide-free (translucent colors) and ATP-bound (solid colors) conformations of the EttA monomer superimposed via least-squares alignment of ABC2. The nucleotide-free conformation represents one ABC1–ABC2 domain pair from the crystallographically observed EttA dimer (**b**), and the ATP-bound conformation was modeled by rigid-body rotations to align the crystallographically observed nucleotide-free conformations of ABC1 and ABC2 to the two protomers in the ATP-sandwich dimer of the E171Q mutant of MJ0796 (details of structural superposition in Online Methods). (**d**) Schematics of the EttA dimer (top), nucleotide-free monomer (middle) and modeled ATP-bound monomer (bottom), colored as above.

(**Supplementary Fig. 1**). Structural superposition demonstrates that ABC1 and ABC2 of EttA are slightly more closely related to each other than to other ABC domains but that they are not more closely related to eEF3 and ABCE1 than to several transmembrane transporters (**Supplementary Table 1**).

As previously observed in other nucleotide-free ABC superfamily structures[32,33], ABC1 and ABC2 of EttA interact in an 'open' conformation in which their ATP-binding sites are both positioned in a deep groove at their mutual interface. However, the Walker A and LSGGE motifs are too far apart to tightly encapsulate ATP in the inter-ABC interface. Their F1-like ATP-binding cores would need to rotate by 44° (as modeled in **Fig. 2c** and **Supplementary Fig. 3a**) to bring them into the closed, catalytically active ATP-sandwich dimer conformation adopted by ABC domains upon binding ATP[3–5]. Furthermore, within each domain, the ABCα subdomain is rotated away from its ATP-binding core by 18–20° relative to the canonical ATP-binding conformation (**Supplementary Fig. 3b**,**c**). The observed deviations from this conformation are all characteristic of nucleotide-free ABC-domain structures[34,35].

The 81-residue linker between the ABC domains in EttA is a unique feature of ABC-Fs that Pfam[22] identifies as conserved domain PF12848. We designate it as the 'P-site tRNA-interaction motif' (PtIM) on the basis of the cryo-EM structure of ribosome-bound EttA[30], which shows a monomer of EttA making extensive interactions with the ribosomal E site and an initiator tRNA in the ribosomal peptidyl-tRNA–binding (P) site[30]. The first half of the PtIM forms an ~50-Å-long extension of the C-terminal α-helix in the ATP-binding core of ABC1. In the crystal structure of EttA, the second half of the PtIM forms a pair of shorter α-helices that pack onto ABC2 (**Fig. 2a**,**b** and **Supplementary Fig. 4a**). These α-helices are followed by seven residues (residues 311–317) that pack into a deep groove between the ABCα and F1-like core subdomains of ABC2 on the surface opposite its interface with ABC1. (We describe possible functional implications of this interaction in **Supplementary Fig. 4b**.)

Approximately 3,500 Å^2 of solvent-accessible surface area per protomer is buried in the interface of the domain-swapped dimer of EttA in the asymmetric unit of its crystal structure (**Fig. 2a**). One-quarter of this interface (~920 Å^2) comes from a reciprocal packing interaction between the first α-helix in the PtIM in each of the two protomers, and this interaction prevents the PtIM in the EttA dimer from adopting the α-helical hairpin configuration that interacts with ribosomes[30] (**Supplementary Fig. 4**). A single rigid-body rotation simultaneously brings the ATP-binding cores of both ABC1–ABC2 domain pairs into the canonical ATP-sandwich conformation (**Supplementary Fig. 3d**). This result suggests that the EttA dimer might be able to bind four ATP molecules cooperatively, although experimental evidence of such cooperativity has not yet been obtained. This dimer could represent an inactive form that buffers the active monomer pool at high EttA concentrations, but further investigation will be required to understand whether the dimer has a physiological function.

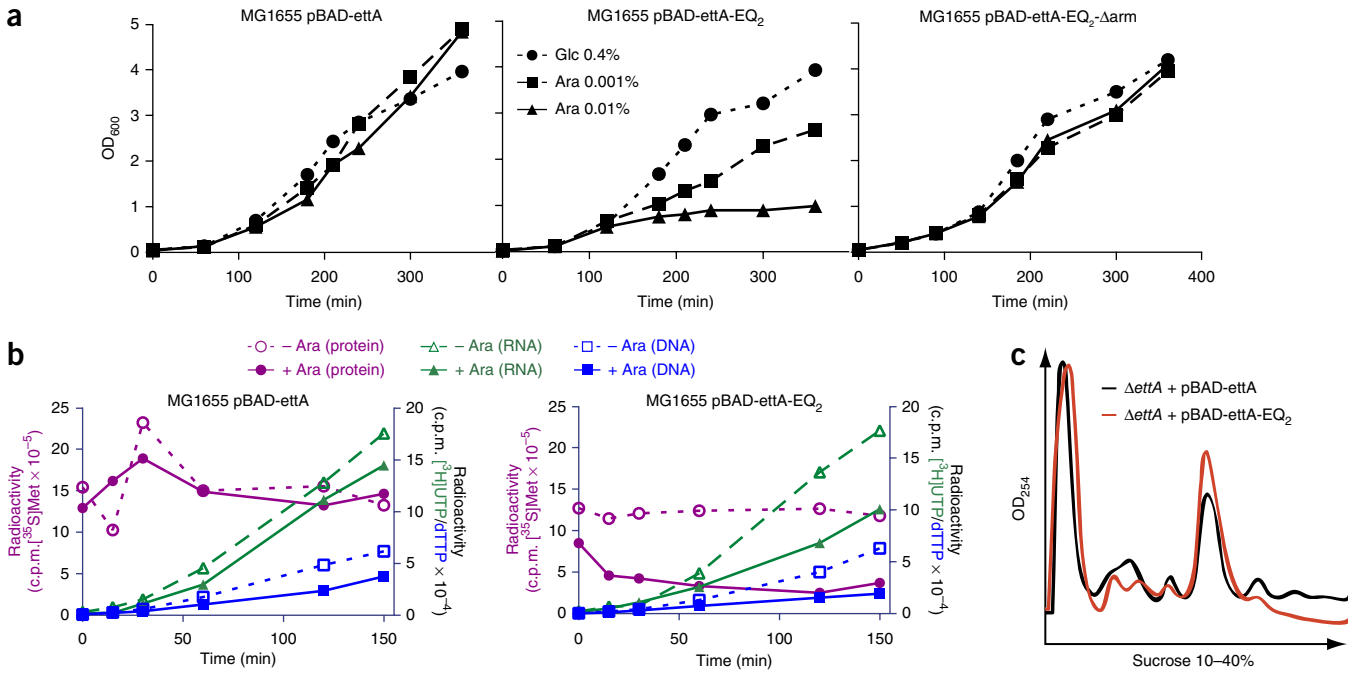

Figure 3 Expression of EttA-EQ_2 causes *trans*-dominant toxicity *in vivo*, because of inhibition of protein synthesis. (**a**) Graphs showing optical density (OD_{600}) profiles during expression of EttA variants in *E. coli* MG1655 in LB medium at 37 °C. Samples are cells containing pBAD-ettA, pBAD-ettA-EQ_2 or pBAD-ettA-EQ_2-Δarm plasmids, grown overnight in LB with 0.4% (w/v) glucose (Glc) to repress EttA expression and then diluted 1:100 into the same medium or one containing 0.001–0.01% (w/v) arabinose (Ara) to induce increasing levels of expression. (**b**) Graphs showing results from experiments using radiolabeled precursors to characterize the influence of expressing EttA variants on protein, RNA and DNA synthesis *in vivo*. Samples are MG1655 cells containing pBAD-ettA or pBAD-ettA-EQ_2 plasmids, grown at 37 °C in M9 glycerol minimal medium to OD_{600} ~0.2 before induction of EttA expression with 0.2% (w/v) Ara at the zero time point. Radioactivity of RNA or DNA labeled by addition of [^{3}H]UTP (green) or [^{3}H]dTTP (blue), respectively, at the same time as the inducer, and of protein labeled at the indicated time points by a 1-min pulse with [^{35}S]methionine (purple) is plotted. (**c**) Plots of sucrose-gradient profiles of polysomes from MG1655 Δ*ettA* cells containing pBAD-ettA or pBAD-ettA-EQ_2 plasmids induced with 0.1% Ara for 30 min after reaching an OD_{600} of 0.6.

EttA-EQ_2 stops cell growth by inhibiting protein synthesis

Guided by the crystal structure, we designed two EttA mutants for physiological studies. EttA-EQ_2 contains dual glutamate-to-glutamine substitutions in the catalytic bases following the Walker B motifs in both ABC domains (Glu188 and Glu470). On the basis of results with other ABC ATPases[5,33,36], these substitutions prevent ATP hydrolysis and trap EttA in its ATP-bound conformation. The other designed mutant, EttA-Δarm, deletes the arm motif, a unique structural feature in ABC1 of ABC-Fs. We used a tightly controlled arabinose-dependent promoter to induce expression of EttA-EQ_2 in *E. coli* MG1655 cells, which resulted in arrest of growth either in the absence (**Fig. 3a**) or presence (data not shown) of a deletion of the endogenous *ettA* (official symbol *yjjK*) gene. In contrast, induction of wild-type EttA (WT EttA), EttA-Δarm or EttA-Δarm-EQ_2 had no effect on growth. Abrogation of the toxicity of EttA-EQ_2 upon deletion of the arm supports our inference that this motif contributes to ABC-F function.

In vivo pulse-chase experiments using radiolabeled substrates for protein synthesis, RNA transcription or DNA replication demonstrate that induction of EttA-EQ_2 rapidly inhibits protein synthesis (**Fig. 3b**). The slower and weaker inhibition of synthesis of RNA and DNA suggests that these effects are secondary to inhibition of protein synthesis. Indeed, purified EttA-EQ_2, but not WT EttA, EttA-Δarm or EttA-Δarm-EQ_2, inhibited *in vitro* translation of a luciferase reporter mRNA (**Supplementary Fig. 6a**,**b**). Immunoblot analyses of fractions from sucrose density gradient ultracentrifugation of ribosomes from *E. coli* MG1655 cells (**Supplementary Fig. 5b**) showed that endogenous WT EttA cofractionates with both 70S ribosomes (monosomes) and polyribosomes (polysomes). Equivalent analyses conducted 30 min after induction of EttA-EQ_2 revealed a decrease in polysomes relative to monosomes (**Fig. 3c**). These observations suggest that the ATP-bound conformation of EttA, as trapped by the EQ_2 mutations, inhibits protein synthesis after formation of the 70S ribosomal initiation complex (70S IC) but before its entry into the elongation cycle. *In vitro* translation experiments on a single mRNA using radiolabeled [^{35}S]methionine support this conclusion (**Supplementary Fig. 6c**).

EttA-EQ_2–ATP traps ribosomes after formation of the first peptide bond

We used a purified *in vitro* translation system[37] to demonstrate that EttA-EQ_2 specifically inhibits protein synthesis after formation of the first peptide bond (**Fig. 4** and **Supplementary Fig. 7**). We preformed a 70S IC by incubating translation initiation factors 1, 2 and 3 with 70S ribosomes, then adding a model mRNA and subsequently [^{35}S]fMet-$tRNA^{fMet}$. The model mRNA, previously used for enzymological studies of ribosome-catalyzed protein synthesis[37,38], contains a Shine–Dalgarno sequence, initial codons encoding an fMet-Phe-Lys-Glu (fMFKE) tetrapeptide and 16 additional codons to fill the ribosomal mRNA-binding channel. After 70S IC formation, we conducted translation elongation reactions in a buffer containing 0.6 mM ATP in addition to 1 mM GTP, the latter nucleotide being required for proper function of elongation factors EF-Tu and EF-G. We analyzed reaction products by using electrophoretic thin-layer chromatography (eTLC), which separates unreacted [^{35}S]fMet amino acid substrate and di-, tri- and tetrapeptide products[39].

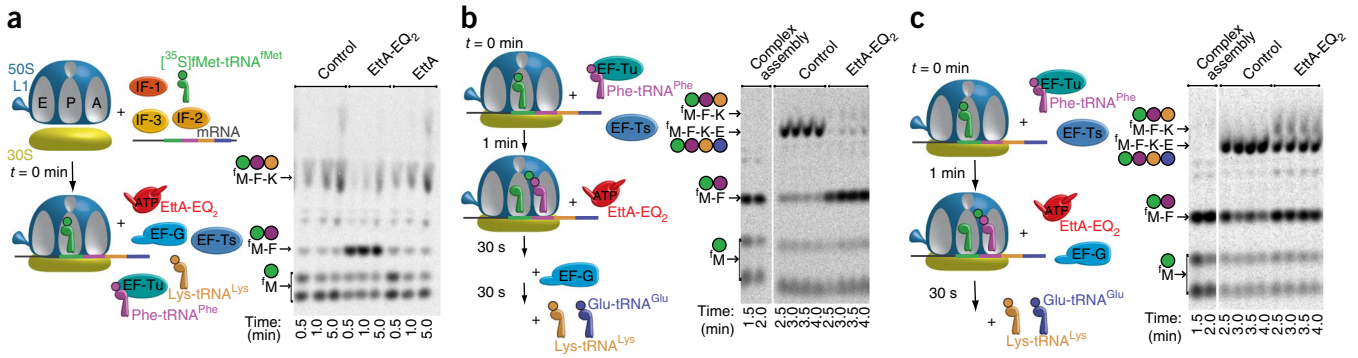

Figure 4 EttA-EQ_2 inhibits translation after formation of the first peptide bond. (**a**–**c**) Autoradiograms (right) of eTLC plates used to separate reaction products from minimum *in vitro* translation assays performed as illustrated in the schematics (left), using an mRNA template encoding an fMet-Phe-Lys-Glu (fMFKE) tetrapeptide. Assays were conducted at 37° C in Polymix buffer containing 3.5 mM $Mg(OAc)_2$, 0.5 mM ATP, 1.0 mM GTP and a phosphoenolpyruvate-based energy-regenerating system. As indicated in the schematics, in **a**, after 70S IC formation, either buffer or 2.5 μM WT EttA or EttA-EQ_2 was added in parallel with the elongation factors, Phe-$tRNA^{Phe}$ and Lys-$tRNA^{Lys}$. In **b**, after formation of the 70S IC and subsequent addition of EF-Tu, EF-Ts and Phe-$tRNA^{Phe}$ to drive synthesis of the first peptide bond, either buffer or EttA-EQ_2 was added 1 min later, and the reaction proceeded for 30 s before addition of EF-G, Lys-$tRNA^{Lys}$ and Glu-$tRNA^{Glu}$ to enable tetrapeptide synthesis. In **c**, the same protocol as in **b** was used, but, to determine whether EF-G and EttA-EQ_2 kinetically compete, EF-G was added in parallel with buffer or EttA-EQ_2 1 min after addition of EF-Tu, EF-Ts and Phe-$tRNA^{Phe}$; 30 s later, Lys-$tRNA^{Lys}$ and Glu-$tRNA^{Glu}$ were added to enable tetrapeptide synthesis. Uncropped images are shown in **Supplementary Figure 9**.

We performed tripeptide synthesis in reactions initiated by addition of a mixture containing EF-Tu, EF-Ts, Phe-$tRNA^{Phe}$ and Lys-$tRNA^{Lys}$ to the preformed 70S IC and subsequent addition of EF-G (**Fig. 4a**). When EttA is omitted or WT EttA is added at the same time as EF-G, an fMFK tripeptide is synthesized efficiently before the translating ribosome stalls at the fourth codon, owing to the absence of a cognate Glu-$tRNA^{Glu}$ (**Fig. 4a**). In contrast, addition of EttA-EQ_2 at the same time as EF-G strongly inhibits translation elongation after formation of the first peptide bond, thus resulting in a reduction in fMFK tripeptide yield and accumulation of fMF dipeptide (**Fig. 4a**). This observation reveals that EttA-EQ_2, which should be locked in the ATP-bound conformation, blocked translation after the first aminoacyl-tRNA was incorporated into the A site and participated in peptide-bond formation at the peptidyl transferase center (PTC) but before a second round of peptide-bond formation. We obtained the same result when EttA-EQ_2 was added before 70S IC formation (**Supplementary Fig. 7a**), demonstrating that 70S IC formation is not inhibited by EttA-EQ_2.

We used variations in the assay protocol to pinpoint the step at which EttA-EQ_2 inhibits the elongation cycle. To test whether inhibition occurs before the first round of EF-G–catalyzed translocation[40,41] on the mRNA template, we varied the order of addition of the components needed to elongate the fMF dipeptide (**Fig. 4b**,**c** and **Supplementary Fig. 7b**), which accumulates in a reaction that proceeds for 1 min in the absence of EF-G and Lys-$tRNA^{Lys}$ (**Fig. 4b**,**c**). Subsequent addition of EF-G together with Lys-$tRNA^{Lys}$ and Glu-$tRNA^{Glu}$ resulted in extension of the fMF dipeptide into an fMFKE tetrapeptide (**Fig. 4b**,**c**), thus demonstrating that the fMF dipeptide product remains covalently attached to $tRNA^{Phe}$ in the A site of the ribosomal pretranslocation complex. Addition of EttA-EQ_2 before EF-G, Lys-$tRNA^{Lys}$ and Glu-$tRNA^{Glu}$ showed almost complete inhibition of the extension of the fMF dipeptide (**Fig. 4b**). In contrast, we observed much weaker inhibition when EttA-EQ_2 was added simultaneously with (**Fig. 4c**) or subsequently to (**Supplementary Fig. 7b**)

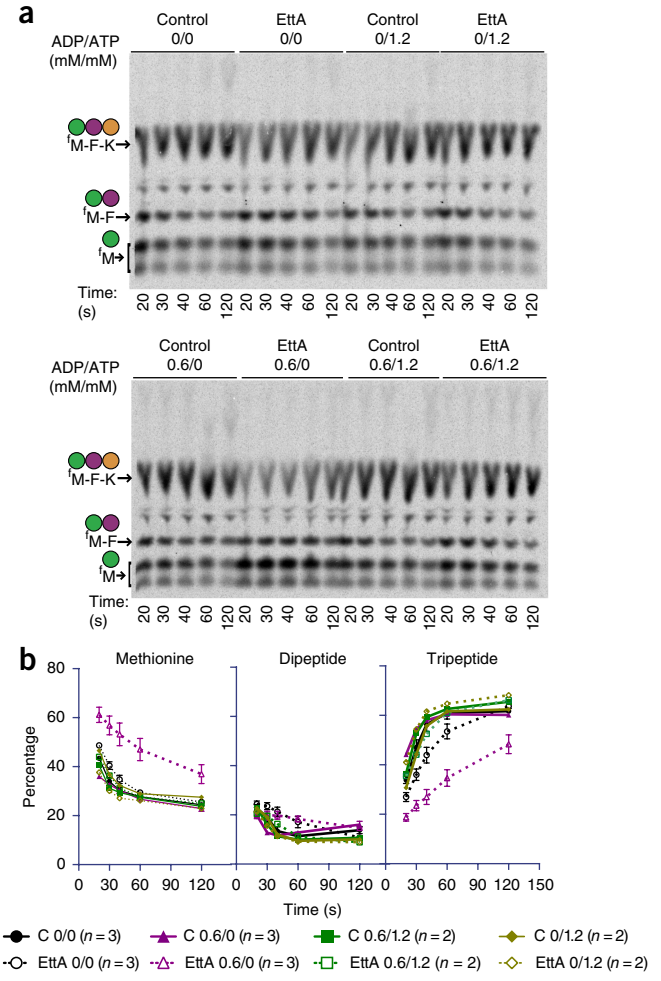

Figure 5 WT EttA inhibits synthesis of the first peptide bond at low ATP/ADP ratio. (**a**) Room-temperature *in vitro* translations with or without 0.6 mM ADP and 1.2 mM ATP, analyzed by eTLC. Reactions, conducted as in **Figure 4a** but with the 70S IC desalted in Polymix buffer, contained 0.3 mM GTP, 0.6 μM 70S ribosomes and, when indicated, 3.5 μM of WT EttA added in parallel with the elongation factors, Phe-$tRNA^{Phe}$ and Lys-$tRNA^{Lys}$. (**b**) Quantification of products in the autoradiograms in **a** with ImageQuant software. Error bars (s.e.m.) are shown only for conditions with $n = 3$ technical replicates.

EF-G, Lys-tRNA^{Lys} and Glu-tRNA^{Glu}. These results demonstrate that EttA-EQ$_2$ and EF-G kinetically compete for interaction with the ribosomal pretranslocation complex carrying deacylated tRNA^{fMet} in the P site and fMF-tRNA^{Phe} in the A site.

Remarkably, fMFKE-tetrapeptide synthesis reactions do not show accumulation of fMFK tripeptide, even when ~50% of fMFKE synthesis is inhibited by EttA-EQ$_2$ (**Fig. 4c** and **Supplementary Fig. 7b**). Therefore, although it strongly inhibits extension of the fMF dipeptide into an fMFK tripeptide, EttA-EQ$_2$ does not significantly inhibit extension of the fMFK tripeptide into an fMFKE tetrapeptide. These observations demonstrate that EttA-EQ$_2$ is specific for ribosomal complexes that have cleared the initiation stage of protein synthesis but have not yet undergone the first round of EF-G–catalyzed translocation[40,41].

EttA prevents peptide-bond formation in the presence of ADP

We further varied the assay protocol to evaluate whether WT EttA's activity is influenced by alterations in ATP/ADP ratio, a parameter that tracks cellular energy supply. WT EttA, like most ABC ATPases[42], interacts in an approximately equivalent manner with A and G nucleotides (unpublished data, G.B. and J.F.H.), whereas the essential GTPase translation factors are specific for G[43]. Therefore, we reduced the concentration of GTP used in our *in vitro* translations from 1 mM to 300 μM so as to enable the addition of physiologically relevant concentrations of ADP and ATP to produce substantial variations in the ratio of nucleotide triphosphates (NTPs) to nucleotide diphosphates (NDPs). (We use the term ATP/ADP ratio in this manuscript as shorthand for the NTP/NDP ratio because these ratios track each other in *E. coli*[44–48]).

WT EttA produces a small, but reproducible, stimulation of fMFK formation in tripeptide synthesis assays in 300 μM GTP and 1.2 mM ATP (**Fig. 5a**). In contrast, WT EttA produces an appreciable kinetic inhibition of formation of fMK dipeptide and fMFK tripeptide in equivalent assays in the presence of the same concentration of GTP but with 0.6 mM ADP substituted for 1.2 mM ATP (**Fig. 5a**,**b**). Because dipeptide synthesis must precede tripeptide synthesis, and WT EttA kinetically inhibits both, we infer that the protein inhibits fMF dipeptide synthesis in the presence of ADP. These results contrast with those presented above demonstrating that, in the presence of ATP, EttA-EQ$_2$ allows fMF dipeptide synthesis while specifically inhibiting fMFK tripeptide synthesis (**Fig. 4**). Analysis of our cryo-EM structure[30] confirms that ribosome-bound EttA-EQ$_2$ is trapped in an ATP-bound conformation in the presence of ATP. Therefore, the contrasting results observed in our *in vitro* translation experiments conducted with WT EttA–ADP compared to EttA-EQ$_2$–ATP indicate important differences in the functional interactions of EttA with translating ribosomes, depending on the relative concentrations of ADP versus ATP.

This inference is supported by single-molecule fluorescence resonance energy transfer (smFRET) experiments showing modest but statistically significant differences in the influence of EttA on the structure and dynamics of the ribosomal L1 stalk in the presence of ADP versus ATP (**Supplementary Fig. 8**). These experiments used a donor fluorophore at the base of the L1 stalk and an acceptor fluorophore at its apical tip (smFRET$_{L1\text{-}L9}$)[49]. In the presence of ATP, EttA-EQ$_2$ increases the mean FRET efficiency (E_{FRET}), thus suggesting a decrease in mean donor-acceptor separation consistent with our cryo-EM structure[30]. WT EttA produces a similar but smaller increase in E_{FRET} in the presence of ATP, presumably reflecting a mixed population of free and EttA-bound 70S ICs, owing to transient interaction of ATP-bound EttA before dissociation induced by ATP hydrolysis. In contrast, in the presence of ADP, WT EttA produces a small decrease in E_{FRET}, thus suggesting an increase in mean donor-acceptor separation. This change in E_{FRET} in the opposite direction from that observed in the presence of ATP demonstrates that EttA modulates the structure or dynamics of the L1 stalk differently in the presence of ATP versus ADP.

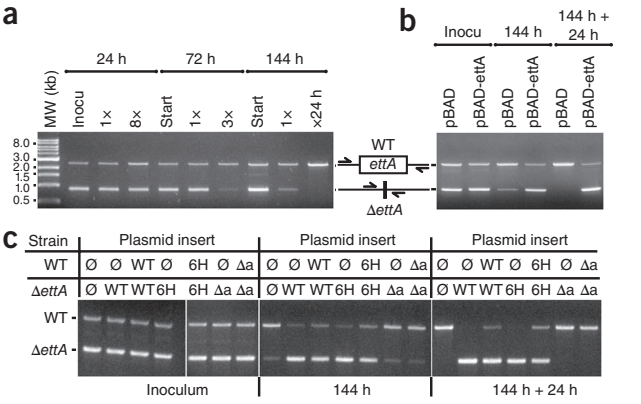

Figure 6 WT and His$_6$-EttA promote survival in long-term stationary phase. (**a**,**b**) Agarose gels of PCR products amplifying the chromosomal region flanking *ettA* by 400 bp, quantifying the relative population of wild-type versus Δ*ettA* cells in competitive fitness assays in LB at 37 °C. (**a**) Samples are starting cultures containing a 1:1 mixture of overnight cultures from the individual strains, grown for 24, 72 or 144 h before reinoculation into fresh medium and regrowth for the same period of time. Eight growth cycles were performed for the 24-h culture, three for the 72-h culture and two for the 144-h culture, which was regrown for an additional 24 h before analysis. MW, molecular weight; inocu, inoculum. (**b**) Samples are mixed cultures of the Δ*ettA* strain containing pBAD or pBAD-ettA plasmids, grown for 144 h before reinoculation for an additional 24 h. (**c**) Results from equivalent complementation experiments performed on mixed cultures of the Δ*ettA* and wild-type strains containing pBAD plasmid with different inserts (ø, no insert; WT, WT EttA; 6H, His$_6$-EttA; Δa, EttA-Δarm). Uncropped images are shown in **Supplementary Figure 9**.

Importantly, inhibition of protein synthesis by WT EttA in the presence of 0.6 mM ADP is relieved when 1.2 mM of protein synthesis ATP is simultaneously included in *in vitro* translation reactions (**Fig. 5a**). Therefore, the ADP/ATP ratio controls WT EttA activity, and a super-stoichiometric ratio of ATP relieves ADP-dependent inhibition of protein synthesis by EttA. These observations suggest that an elevated cellular ADP/ATP ratio, as found in energy-depleted cells[44,50], will cause EttA to stabilize 70S ICs in a 'hibernating' conformation that prevents commitment of metabolic resources to synthesis of incomplete proteins. This hypothesis, based on our *in vitro* enzymological studies, suggests that EttA could have a substantial role in controlling protein synthesis in stationary-phase cells, in which the rates of protein synthesis and cell growth[51–54] decline, owing to depletion of nutritional and energetic resources.

Δ*ettA* impairs fitness in long-term stationary phase

Consistently with this hypothesis, western blots demonstrate that EttA expression increases in stationary phase (**Supplementary Fig. 5c**), when there is a declining ATP/ADP ratio[44,50,53]. Increasing expression should promote formation of EttA-bound, hibernating 70S ICs poised to rapidly resume protein synthesis when energy, in the form of ATP, becomes available again. Therefore, we investigated whether EttA influences fitness when growth in fresh LB medium is resumed out of stationary phase. Indeed, Δ*ettA E. coli* exhibited a progressively more severe competitive disadvantage as we extended residency in stationary phase from 1 to 6 d (**Fig. 6a**) before restarting growth. This defect was complemented by expression of WT EttA or hexahistidine (His$_6$)-EttA (**Fig. 6b**,**c**) but not EttA-Δarm (**Fig. 6c**).

The parallel effects of the Δarm mutation in abrogating the inhibition of *in vitro* translation by EttA-EQ_2 and in eliminating the *in vivo* fitness advantage conferred by WT EttA supports the hypothesis that this advantage derives from the functional interaction of EttA with ribosomes.

DISCUSSION

Our biochemical results demonstrate that EttA, the most widely distributed ABC-F protein among eubacteria, is a new translation factor that controls the progression of 70S ICs into the translation elongation cycle by using a mechanism sensitive to the ATP/ADP ratio. We also present genetic experiments showing that knockout of the *ettA* gene produces a severe fitness defect in *E. coli* in long-term stationary phase (**Fig. 6**). This observation supports the hypothesis that EttA contributes to regulating the commitment of metabolic resources to protein synthesis and to preventing the synthesis of incomplete proteins in energy-depleted cells.

Our results, combined with those in ref. 30 and published work on ABC ATPases[3–5], support a straightforward model for the interaction of ATP-bound EttA with the 70S IC (**Fig. 7**), although several alternative models outlined below could explain the more complex influence of ADP on this interaction. The ATP-hydrolysis cycle of ABC ATPases, like that of other NTPases, involves orderly progression through a series of conformational states coupled to ATP binding, ATP hydrolysis and release of the products (ADP and inorganic phosphate). As observed for other ABC ATPases[3–5], EttA's two ABC domains adopt an open conformation in the absence of bound nucleotide, as visualized in our nucleotide-free X-ray crystal structure of WT EttA (**Fig. 1a**,**b**) in which the ATP-binding site in each ABC domain faces the other ABC domain without directly contacting it (**Fig. 1a**,**b**). Binding of two ATP molecules to these sites closes the interface between the ABC domains to produce a more compact conformation with greatly increased affinity for the 70S IC, as visualized in the cryo-EM structure of ATP-bound EttA-EQ_2 reported in ref. 30. This structure shows EttA bound in the E site of the ribosome, where its arm motif contacts the L1 stalk of the large ribosomal subunit, and its PtIM interacts with the acceptor stem of a P-site–bound deacylated initiator $tRNA^{fMet}$. The small but reproducible stimulation of dipeptide synthesis by WT EttA in the presence of ATP (**Fig. 5**) suggests that ATP-bound EttA stabilizes the ribosome in a conformation that promotes peptide-bond formation in the PTC. Interaction with the ribosome, in turn, stimulates ATP hydrolysis by EttA (**Supplementary Fig. 5b**), and this reaction triggers release of EttA from the ribosome and entry of the ribosome into the translation elongation cycle. By blocking ATP hydrolysis, the EQ_2 mutations in EttA trap the protein in the otherwise transient ATP-bound state and consequently block its release from the ribosome. In WT EttA, transient electrostatic forces generated during ATP hydrolysis may accelerate this release process. Once engaged in the translation elongation cycle, the ribosome becomes resistant to the rebinding of EttA (**Fig. 4** and **Supplementary Fig. 6c**), presumably either owing to EttA having reduced affinity for elongator tRNAs compared to the initiator $tRNA^{fMet}$ in the P site or owing to deacylated tRNAs passing through and blocking the E site as they exit the translating ribosome.

Our data show that WT EttA has a qualitatively different effect on translation in the presence of ADP compared to the effects of either WT EttA or EttA-EQ_2 in the presence of ATP (**Figs. 4** and **5**). In the presence of ADP, WT EttA inhibits synthesis of the first peptide bond by the 70S IC rather than promoting this reaction or trapping its product, as observed in the presence of ATP for WT EttA and EttA-EQ_2, respectively. Several models could explain this alternative activity in the presence of ADP compared to ATP. One possibility is that ADP interacts with the ribosome to alter its interaction with EttA, whereas an alternative possibility is that ADP binds to one or both of the ATPase active sites in EttA, thus resulting in an altered conformation that still binds to the 70S IC but stabilizes it in a conformation that inhibits rather than promotes formation of the first peptide. There are several possible explanations for the different behavior of EttA upon direct binding of ADP compared to its behavior in the posthydrolysis complex with ADP formed after binding and hydrolyzing ATP. A related mechanistic issue concerns the question of whether there is functional asymmetry between the two ATPase active sites in EttA. These issues are addressed in the **Supplementary Note**.

Additional studies will be required to understand how EttA interacts with other cellular systems regulating protein synthesis in stationary phase. A key contributor is likely to be the coupled reductions in GTP/GDP and ATP/ADP ratios in energy-depleted cells (a phenomenon mediated by the phosphotransferase activities of nucleoside diphosphate kinase and adenylate kinase[45–48]). GDP exerts strong feedback inhibition of most of the essential GTPase translation factors[55], and this effect will reduce the rates of both initiation and elongation in energy-depleted cells. This baseline metabolic effect should amplify the activity of EttA and the other proteins that modulate

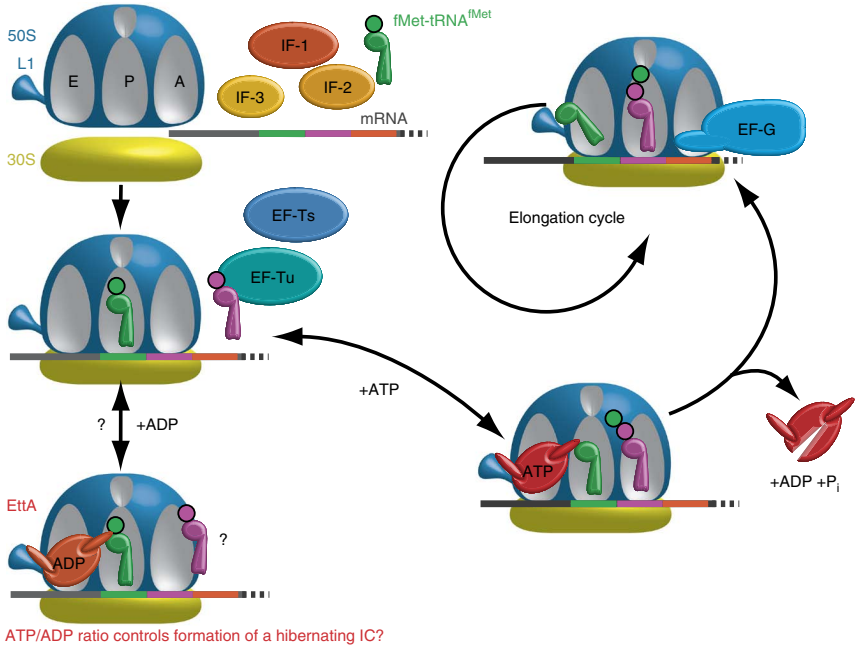

Figure 7 Schematic model of EttA function based on the results presented here and in ref. 30. In the presence of ADP, EttA inhibits formation of the first peptide bond (**Fig. 5b**); this may be mediated by stabilization of the 70S IC in a hibernating state by ADP-bound EttA (described in main text). In contrast, ATP-bound EttA stimulates the formation of the first peptide bond by the ribosome and then, concomitantly with ATP hydrolysis, dissociates from the ribosome, thereby allowing it to enter the elongation cycle. P_i, inorganic phosphate.

protein translation in stressed and energy-depleted cells. These include some toxin-antitoxin systems[56,57], the ribosomal silencing factor[58] (RsfA) protein and the ribosome modulation factor (RMF) protein[59,60]. Toxin-antitoxin systems improve survival under stress conditions by inhibiting critical physiological processes including protein synthesis[57]. RsfA, which has a phylogenetic distribution as broad as that of EttA, inhibits translation in stationary phase by preventing the joining of the large and small ribosomal subunits to form the 70S IC[58]. RMF, which has a narrow phylogenetic distribution that is limited to proteobacteria, drives dimerization of 70S ribosomes in stationary phase to form inactive 100S diribosome complexes[59,60]. Although experiments focused on each of these factors individually have shown that they can contribute to controlling protein synthesis in energy-depleted cells, the manner in which they interact under different metabolic and environmental conditions is not understood.

The biochemical properties of EttA raise intriguing possibilities for regulation of protein synthesis in response to such environmental variations. The observation that EttA targets a 70S IC poised to translate a bound mRNA suggests that it could act preferentially on mRNAs encoding specific target proteins[18], whereas specificity seems unlikely for the other factors that regulate protein synthesis in energy-depleted cells. If EttA does have such specificity, its activity inhibiting entry into the translational elongation cycle at high ADP concentration (**Fig. 5**) can attenuate the expression of specific proteins under conditions of energy depletion while simultaneously preparing them for rapid synthesis when energy levels return to normal. Such targeted hibernation activity would enable EttA and potentially other ABC-Fs[18] to influence cellular fitness not only under conditions of energy deprivation but also in an anticipatory manner upon resumption of growth. ABC-Fs could thereby provide a powerful mechanism for differential control of the translation of specific proteins not only under conditions of growth limitation but also at the time of growth reinitiation. In this context, we note that, in the presence of ATP, *E. coli* YbiT-EQ$_2$ interacts with ribosomes *in vitro* in a similar manner to that of EttA-EQ$_2$ (unpublished data, G.B., R.L.G. and J.F.H.).

Our results establish a technical foundation for broader and deeper studies of ABC-F proteins. The fact that these proteins have evaded detailed functional characterization until now, despite their great phylogenetic prevalence and diversity, suggests that substantial gaps remain in understanding of the physiology and systems biology of protein synthesis.

METHODS

Methods and any associated references are available in the online version of the paper.

Accession codes. Coordinates of the X-ray structure of EttA have been deposited in the Protein Data Bank, under accession code 4FIN.

Note: Any Supplementary Information and Source Data files are available in the online version of the paper.

ACKNOWLEDGMENTS

This work was supported by US National Science Foundation grants to J.F.H. (0424043) and R.L.G. (MCB CAREER 0644262), a Burroughs Wellcome Fund award to R.L.G. (CABS 1004856), a Canadian Institutes of Health Research grant to H.-J.W. (MOP 114938), a grant from the US National Institutes of Health (NIH) Protein Structure Initiative to the Northeast Structural Genomics Consortium (GM074958) and NIH grants to R.L.G. (GM084288) and to J.F. (GM29169 and GM55440). M.T.E. was supported by the NIH Training Program in Molecular Biophysics at Columbia University (T32 GM008281). J.F. is supported as an Investigator by the Howard Hughes Medical Institute. The authors thank J. Hurley and N. Woychik of the University of Medicine and Dentistry of the State of New Jersey for assistance with *in vivo* radiolabeling, A. Tzagoloff for sharing equipment and the members of the Hunt and Gonzalez laboratories for advice and technical assistance.

AUTHOR CONTRIBUTIONS

P.C.S. determined the crystal structure and performed the polysome analysis of WT EttA. J.J.F. performed the ATPase measurements. G.B., with assistance from A.J.T., performed the other biochemical and genetic studies. W.N. performed the smFRET experiments. M.T.E. provided training and reagents for *in vitro* translation assays and eTLC analysis of *in vitro* translation products. B.C., Y.H. and J.F. determined in the cryo-EM structure of ribosome-bound EttA-EQ$_2$. G.B., P.C.S., H.-J.W., R.L.G. and J.F.H. designed the experiments. G.B., P.C.S., B.C., J.F., R.L.G. and J.F.H. conceived the research program and wrote the manuscript.

COMPETING FINANCIAL INTERESTS

The authors declare no competing financial interests.

1. Davidson, A.L., Dassa, E., Orelle, C. & Chen, J. Structure, function, and evolution of bacterial ATP-binding cassette systems. *Microbiol. Mol. Biol. Rev.* **72**, 317–364 (2008).
2. Cavanaugh, L.F., Palmer, A.G. III, Gierasch, L.M. & Hunt, J.F. Disorder breathes life into a DEAD motor. *Nat. Struct. Mol. Biol.* **13**, 566–569 (2006).
3. Jones, P.M. & George, A.M. Subunit interactions in ABC transporters: towards a functional architecture. *FEMS Microbiol. Lett.* **179**, 187–202 (1999).
4. Hopfner, K.P. *et al.* Structural biology of Rad50 ATPase: ATP-driven conformational control in DNA double-strand break repair and the ABC-ATPase superfamily. *Cell* **101**, 789–800 (2000).
5. Smith, P.C. *et al.* ATP binding to the motor domain from an ABC transporter drives formation of a nucleotide sandwich dimer. *Mol. Cell* **10**, 139–149 (2002).
6. Holland, I.B. & Blight, M.A. ABC-ATPases, adaptable energy generators fuelling transmembrane movement of a variety of molecules in organisms from bacteria to humans. *J. Mol. Biol.* **293**, 381–399 (1999).
7. Jaciuk, M., Nowak, E., Skowronek, K., Tanska, A. & Nowotny, M. Structure of UvrA nucleotide excision repair protein in complex with modified DNA. *Nat. Struct. Mol. Biol.* **18**, 191–197 (2011).
8. Lammens, K. *et al.* The Mre11:Rad50 structure shows an ATP-dependent molecular clamp in DNA double-strand break repair. *Cell* **145**, 54–66 (2011).
9. Skogerson, L. & Wakatama, E. A ribosome-dependent GTPase from yeast distinct from elongation factor 2. *Proc. Natl. Acad. Sci. USA* **73**, 73–76 (1976).
10. Khoshnevis, S. *et al.* The iron-sulphur protein RNase L inhibitor functions in translation termination. *EMBO Rep.* **11**, 214–219 (2010).
11. Pisarev, A.V. *et al.* The role of ABCE1 in eukaryotic posttermination ribosomal recycling. *Mol. Cell* **37**, 196–210 (2010).
12. Barthelme, D. *et al.* Ribosome recycling depends on a mechanistic link between the FeS cluster domain and a conformational switch of the twin-ATPase ABCE1. *Proc. Natl. Acad. Sci. USA* **108**, 3228–3233 (2011).
13. Becker, T. *et al.* Structural basis of highly conserved ribosome recycling in eukaryotes and archaea. *Nature* **482**, 501–506 (2012).
14. Kamath, A. & Chakraburtty, K. Role of yeast elongation factor 3 in the elongation cycle. *J. Biol. Chem.* **264**, 15423–15428 (1989).
15. Andersen, C.B. *et al.* Structure of eEF3 and the mechanism of transfer RNA release from the E-site. *Nature* **443**, 663–668 (2006).
16. Kurata, S. *et al.* Ribosome recycling step in yeast cytoplasmic protein synthesis is catalyzed by eEF3 and ATP. *Proc. Natl. Acad. Sci. USA* **107**, 10854–10859 (2010).
17. Tyzack, J.K., Wang, X., Belsham, G.J. & Proud, C.G. ABC50 interacts with eukaryotic initiation factor 2 and associates with the ribosome in an ATP-dependent manner. *J. Biol. Chem.* **275**, 34131–34139 (2000).
18. Paytubi, S. *et al.* ABC50 promotes translation initiation in mammalian cells. *J. Biol. Chem.* **284**, 24061–24073 (2009).
19. Kiel, M.C., Aoki, H. & Ganoza, M.C. Identification of a ribosomal ATPase in *Escherichia coli* cells. *Biochimie* **81**, 1097–1108 (1999).
20. Babu, M. *et al.* Ribosome-dependent ATPase interacts with conserved membrane protein in *Escherichia coli* to modulate protein synthesis and oxidative phosphorylation. *PLoS ONE* **6**, e18510 (2011).
21. Kerr, I.D. Sequence analysis of twin ATP binding cassette proteins involved in translational control, antibiotic resistance, and ribonuclease L inhibition. *Biochem. Biophys. Res. Commun.* **315**, 166–173 (2004).
22. Punta, M. *et al.* The Pfam protein families database. *Nucleic Acids Res.* **40**, D290–D301 (2012).
23. Vazquez de Aldana, C.R., Marton, M.J. & Hinnebusch, A.G. GCN20, a novel ATP binding cassette protein, and GCN1 reside in a complex that mediates activation of the eIF-2 alpha kinase GCN2 in amino acid-starved cells. *EMBO J.* **14**, 3184–3199 (1995).

24. Sattlegger, E. & Hinnebusch, A.G. Polyribosome binding by GCN1 is required for full activation of eukaryotic translation initiation factor 2α kinase GCN2 during amino acid starvation. *J. Biol. Chem.* **280**, 16514–16521 (2005).
25. Dong, J., Lai, R., Jennings, J.L., Link, A.J. & Hinnebusch, A.G. The novel ATP-binding cassette protein ARB1 is a shuttling factor that stimulates 40S and 60S ribosome biogenesis. *Mol. Cell Biol.* **25**, 9859–9873 (2005).
26. Hopkins, J.D., Clements, M. & Syvanen, M. New class of mutations in *Escherichia coli* (*uup*) that affect precise excision of insertion elements and bacteriophage Mu growth. *J. Bacteriol.* **153**, 384–389 (1983).
27. Murat, D., Bance, P., Callebaut, I. & Dassa, E. ATP hydrolysis is essential for the function of the Uup ATP-binding cassette ATPase in precise excision of transposons. *J. Biol. Chem.* **281**, 6850–6859 (2006).
28. Murat, D., Goncalves, L. & Dassa, E. Deletion of the *Escherichia coli uup* gene encoding a protein of the ATP binding cassette superfamily affects bacterial competitiveness. *Res. Microbiol.* **159**, 671–677 (2008).
29. Lu, P., Vogel, C., Wang, R., Yao, X. & Marcotte, E.M. Absolute protein expression profiling estimates the relative contributions of transcriptional and translational regulation. *Nat. Biotechnol.* **25**, 117–124 (2007).
30. Chen, B. *et al.* EttA regulates translation by binding to the ribosomal E site and restricting ribosome-tRNA dynamics. *Nat. Struct. Mol. Biol.* doi:10.1038/nsmb.2741 (5 January 2014).
31. Zaitseva, J., Jenewein, S., Jumpertz, T., Holland, I.B. & Schmitt, L. H662 is the linchpin of ATP hydrolysis in the nucleotide-binding domain of the ABC transporter HlyB. *EMBO J.* **24**, 1901–1910 (2005).
32. Karcher, A., Schele, A. & Hopfner, K.P. X-ray structure of the complete ABC enzyme ABCE1 from *Pyrococcus abyssi*. *J. Biol. Chem.* **283**, 7962–7971 (2008).
33. Oldham, M.L. & Chen, J. Crystal structure of the maltose transporter in a pretranslocation intermediate state. *Science* **332**, 1202–1205 (2011).
34. Diederichs, K. *et al.* Crystal structure of MalK, the ATPase subunit of the trehalose/maltose ABC transporter of the archaeon *Thermococcus litoralis*. *EMBO J.* **19**, 5951–5961 (2000).
35. Karpowich, N. *et al.* Crystal structures of the MJ1267 ATP binding cassette reveal an induced-fit effect at the ATPase active site of an ABC transporter. *Structure* **9**, 571–586 (2001).
36. Vergani, P., Lockless, S.W., Nairn, A.C. & Gadsby, D.C. CFTR channel opening by ATP-driven tight dimerization of its nucleotide-binding domains. *Nature* **433**, 876–880 (2005).
37. Fei, J. *et al.* A highly purified, fluorescently labeled *in vitro* translation system for single-molecule studies of protein synthesis. *Methods Enzymol.* **472**, 221–259 (2010).
38. Yusupova, G.Z., Yusupov, M.M., Cate, J.H. & Noller, H.F. The path of messenger RNA through the ribosome. *Cell* **106**, 233–241 (2001).
39. Youngman, E.M., Brunelle, J.L., Kochaniak, A.B. & Green, R. The active site of the ribosome is composed of two layers of conserved nucleotides with distinct roles in peptide bond formation and peptide release. *Cell* **117**, 589–599 (2004).
40. Fei, J., Kosuri, P., MacDougall, D.D. & Gonzalez, R.L. Jr. Coupling of ribosomal L1 stalk and tRNA dynamics during translation elongation. *Mol. Cell* **30**, 348–359 (2008).
41. Agrawal, R.K., Heagle, A.B., Penczek, P., Grassucci, R.A. & Frank, J. EF-G-dependent GTP hydrolysis induces translocation accompanied by large conformational changes in the 70S ribosome. *Nat. Struct. Biol.* **6**, 643–647 (1999).
42. Aleksandrov, A.A., Cui, L. & Riordan, J.R. Relationship between nucleotide binding and ion channel gating in cystic fibrosis transmembrane conductance regulator. *J. Physiol.* (*Lond.*) **587**, 2875–2886 (2009).
43. Ramakrishnan, V. Ribosome structure and the mechanism of translation. *Cell* **108**, 557–572 (2002).
44. Buckstein, M.H., He, J. & Rubin, H. Characterization of nucleotide pools as a function of physiological state in *Escherichia coli*. *J. Bacteriol.* **190**, 718–726 (2008).
45. Glembotski, C.C., Chapman, A.G. & Atkinson, D.E. Adenylate energy charge in *Escherichia coli* CR341T28 and properties of heat-sensitive adenylate kinase. *J. Bacteriol.* **145**, 1374–1385 (1981).
46. Lu, Q. & Inouye, M. Adenylate kinase complements nucleoside diphosphate kinase deficiency in nucleotide metabolism. *Proc. Natl. Acad. Sci. USA* **93**, 5720–5725 (1996).
47. Bernard, M.A., Ray, N.B., Olcott, M.C., Hendricks, S.P. & Mathews, C.K. Metabolic functions of microbial nucleoside diphosphate kinases. *J. Bioenerg. Biomembr.* **32**, 259–267 (2000).
48. Walton, G.M. & Gill, G.N. Nucleotide regulation of protein synthesis. *Methods Enzymol.* **60**, 578–590 (1979).
49. Fei, J., Richard, A.C., Bronson, J.E. & Gonzalez, R.L. Jr. Transfer RNA–mediated regulation of ribosome dynamics during protein synthesis. *Nat. Struct. Mol. Biol.* **18**, 1043–1051 (2011).
50. Tran, Q.H. & Unden, G. Changes in the proton potential and the cellular energetics of *Escherichia coli* during growth by aerobic and anaerobic respiration or by fermentation. *Eur. J. Biochem.* **251**, 538–543 (1998).
51. Swedes, J.S., Sedo, R.J. & Atkinson, D.E. Relation of growth and protein synthesis to the adenylate energy charge in an adenine-requiring mutant of *Escherichia coli*. *J. Biol. Chem.* **250**, 6930–6938 (1975).
52. Jewett, M.C., Miller, M.L., Chen, Y. & Swartz, J.R. Continued protein synthesis at low [ATP] and [GTP] enables cell adaptation during energy limitation. *J. Bacteriol.* **191**, 1083–1091 (2009).
53. Chapman, A.G., Fall, L. & Atkinson, D.E. Adenylate energy charge in *Escherichia coli* during growth and starvation. *J. Bacteriol.* **108**, 1072–1086 (1971).
54. Gaal, T., Bartlett, M.S., Ross, W., Turnbough, C.L. & Gourse, R.L. Transcription regulation by initiating NTP Concentration: rRNA synthesis in bacteria. *Science* **278**, 2092–2097 (1997).
55. Walton, G.M. & Gill, G.N. Regulation of ternary (Met-tRNAf - GTP - eukaryotic initiation factor 2) protein synthesis initiation complex formation by the adenylate energy charge. *Biochim. Biophys. Acta* **418**, 195–203 (1976).
56. Schifano, J.M. *et al.* Mycobacterial toxin MazF-mt6 inhibits translation through cleavage of 23S rRNA at the ribosomal A site. *Proc. Natl. Acad. Sci. USA* **110**, 8501–8506 (2013).
57. Yamaguchi, Y., Park, J.H. & Inouye, M. Toxin-antitoxin systems in bacteria and archaea. *Annu. Rev. Genet.* **45**, 61–79 (2011).
58. Häuser, R. *et al.* RsfA (YbeB) proteins are conserved ribosomal silencing factors. *PLoS Genet.* **8**, e1002815 (2012).
59. Polikanov, Y.S., Blaha, G.M. & Steitz, T.A. How hibernation factors RMF, HPF, and YfiA turn off protein synthesis. *Science* **336**, 915–918 (2012).
60. Yamagishi, M. *et al.* Regulation of the *Escherichia coli rmf* gene encoding the ribosome modulation factor: growth phase- and growth rate-dependent control. *EMBO J.* **12**, 625–630 (1993).

ONLINE METHODS

The **Supplementary Note** documents protein purification, crystallization, methods used in this paper and methods used in the experiments presented in **Supplementary Figures 1–9**.

Bacterial strains. Standard *E. coli* strains for cloning (DH5α) and protein expression (BL21(λDE3) and B834) were obtained from commercial vendors. Strains MG1655 (sequenced WT strain) and FB21853 (MG1655 *yjjK*::Tn*5*) were purchased from the *E. coli* Genome Project at the University of Wisconsin (http://www.genome.wisc.edu/). All other strains were purchased from the *E. coli* Genetic Stock Center at Yale University[61] or constructed in the course of these studies. Genetic and physiological assays were performed with *E. coli* K12 strain MG1655 or derivates. Because we found that strain FB21853 is not isogenic to the sequenced WT strain MG1655, we reconstructed MG1655 *yjjK*::Tn*5* by P1 transduction[62] of the *yjjK*::Tn*5* locus from strain FB21853 into the sequenced WT strain MG1655. The resulting strain, designated *ettA*::Tn*5*, was used for the early phases of the work reported in this paper. The interruption of the *ettA* gene in this strain was verified by western blot with an antibody against the EttA protein (raised as described below). We also built a strain deleted of *yjjK*/*ettA* that did not carry any antibiotic resistance, by using the procedure developed by Datsenko and Wanner[63]. Briefly, the strain deleted for *yjjK* in the Keio collection[64] (JW4354-1, CGSC no. 11108) was used as a template to generate the PCR product to mutate the MG1655 strain by amplification of the yjjK/ettA locus with primers 400 pb upstream and downstream of the locus. This PCR product was electroporated in the MG1655 strain carrying the pKD46, the transformed strain was cured of the pKD46 plasmid and the insertion of the PCR product in the genome at the good locus was verified by PCR. The positive strain was cured of the pKD46 plasmid and transformed with the FLP helper plasmid pCP20. The resulting colonies were screened for the flip-out of the kanamycin marker by PCR. The verified strain was cured of the pCP20 plasmid and used for the fitness experiment. This strain is referred to as Δ*ettA*. All the constructs were verified by PCR and sequencing of the modified locus.

Plasmids. The gene encoding EttA (YjjK) was amplified by PCR with MG1655 genomic DNA as a template with 5′ primer containing the NcoI restriction site and six codons encoding histidine in front of the initiator GTG codon, which was replaced by an ATG codon. The 3′ primer used for this PCR had the stop codon of *yjjK* followed by an XhoI restriction site. This PCR product was cloned into the pBAD/Myc-HisA vector (Invitrogen) with the restriction enzymes NcoI and XhoI (Fermentas). The resulting plasmid was called pBAD-His_6-ettA. For the plasmid pBAD-ettA, which expressed the native protein without tag, the same procedure was used but with a 5′ primer that does not encode the His_6 tag. The plasmid expressing the EttA E188Q mutant was made by QuikChange II site-directed mutagenesis (Agilent Technologies) with primers that replaced the codon of the Glu188 with a glutamine and used the pBAD-ettA plasmid as template. The resulting plasmid was verified and named pBAD-ettA-E188Q. The plasmid expressing the EttA-EQ_2 was made with the same technique with primers, which replaced the codon of the Glu470 with a glutamine and the pBAD-ettA-E188Q as template; the resulting plasmid was named pBAD-ettA-EQ_2. The deletion of the arm domain (plasmid pBAD-ettA-Δarm) was also done by QuikChange with the pBAD-ettA as template and primer designed to substitute the three-residue sequence GGS for residues 96 to 141 in the native EttA sequence (EVVNALKRLDEVYALYADPDADF DKLAAEQGRLEEIIQAHDGHN LN). The plasmid pBAD-ettA-EQ_2-Δarm was created with the same approach, but with the plasmid pBAD-ettA-EQ_2 as template. The same constructs, expressing a histidine-tagged protein, were made similarly, but with the pBAD-His_6-ettA as starting plasmid. For structure determination, the *yjjK*/*ettA* gene was inserted into vector pET28c (EMD Biosciences) at the NcoI and XhoI restriction sites so as to express the full-length protein with no additional tags or amino acids. All the plasmids were verified by DNA sequencing.

Bacterial growth media. Bacteria were cultivated in LB medium (Affymetrix/USB). Ampicillin was added at 100 μg/ml for cultures containing pBAD-based plasmids. Kanamycin was added at 25 μg/ml for the mutant construct.

Estimation of EttA concentration *in vivo*. The quantitative proteomics study of Lu *et al.*[29] reports the concentration of EttA (YjjK) to be 2,167 molecules per cell during exponential growth in glucose minimal medium, which corresponds to 7 μM protomer (assuming an average cell volume[65] of 4.96×10^{-16} L). We have verified by western blot analysis that the expression level of EttA is similar in exponential phase in glucose minimal medium or LB (unpublished data, G.B. and J.F.H.). The western blot data presented in **Supplementary Figure 5c** shows that EttA expression increases after 24 h of growth, to a level approximately three-fold higher than in exponential phase. Therefore, on the basis of the calibration described above, the EttA concentration in stationary phase is ~21 μM.

Crystallization, X-ray data collection and structure determination. Crystals of EttA (either native or selenomethionine derivatized) regularly exhibited streaked and highly mosaic diffraction. Out of hundreds of crystals screened, a single selenomethionine crystal showed diffraction convincingly beyond 3 Å with a rotating anode X-ray source. Data from this crystal were collected on NSLS beamline X12C with a Brandeis-B4 detector, a Nonius/Bruker diffractometer (c. 1999), an ambient temperature of 130 K and a wavelength corresponding to maximum f′ as measured by an online fluorescence scan (0.97961 Å). A total of 529 frames of 1° oscillation images were processed with DENZO and merged with SCALEPACK with the 'no merge original index' and 'scale anomalous' options[66]. The resulting data set was highly redundant and complete to a limiting resolution of 2.4 Å (**Table 1**) and, on the basis of a solvent content of 50%, was expected to contain two EttA protomers per asymmetric unit. The resulting data set was analyzed with the 'SAD' option in SOLVE version 2.03 (ref. 67) with a limiting resolution of 3.0 Å. The anomalous signal-to-noise ratio for this data set was estimated at only 0.64. Nonetheless, SOLVE identified 18 selenium sites that obeyed two-fold rotational noncrystallographic symmetry (NCS). However, the resulting electron density maps were uninterpretable. Inversion of the site pattern and recalculation of phases, followed by extensive solvent flattening in RESOLVE[68], did produce an interpretable electron density map. The protein model was built by hand with O[69] and initially refined in CNS[70] with standard procedures along with NCS restraints. Further iterative refinement and rebuilding were carried out with PHENIX[71] and Coot[72], respectively. Refinement in PHENIX was carried out with the same set of 'free' reflections as had been used in CNS, but NCS restraints were not applied. The final model of EttA contained 1,065 protein residues in two chains (six alternate conformations), 11 sulfate ions, 1 citrate ion, 1 triethyleneglycol molecule, 9 molecules of glycerol and 396 waters. The model refined to R/R_{free} values of 18.3% and 24.3%, respectively, with a Wilson B factor of 27.7, no Ramachandran outliers, 98.3% and 1.7% of residues in most-favored and additionally allowed regions, and excellent geometry throughout (**Table 1**). The two molecules are related to each other by a rotation of 180° about an axis parallel to the crystallographic C axis. The two protomers differ only slightly when superimposed with an r.m.s. deviation of 1.23 Å for 95% of common atoms. Structural analysis was carried out with CCP4 (ref. 73) and the Uppsala Software Factory suites[74]. Structure figures for EttA were produced in PyMOL (http://www.pymol.org/). Coordinates for *E. coli* EttA are deposited in the Protein Data Bank under accession code 4FIN.

Structural superposition. Alignments in **Figure 2c** were based on least-squares superposition of the ABCβ and F1-like core subdomains in one ABC domain of EttA with one corresponding region of one protomer in the MJ0706 ATP-sandwich dimer[5]. ATP molecules from the MJ0796 dimer are shown in gray space-filling representation.

***In vivo* assays of DNA, RNA and protein synthesis.** MG1655 cells containing pBAD-ettA or pBAD-ettA-EQ_2 plasmids were grown at 37 °C in M9 glycerol minimal medium with 0.1 mg/ml of amino acid (minus methionine and cysteine) to an OD_{600} of ~0.2 before induction of EttA expression with 0.2% L-arabinose (at zero time on these graphs). Control cultures were done the same way without L-arabinose. [^{35}S]methionine incorporation was carried out with the protocol of Hirashima and Inouye[75]. At each time point, 1 ml of each culture was incubated with 6 μl of [^{35}S]methionine for 1 min. The reaction was stopped by addition of 300 μl of cold methionine (0.1 mg/ml).

doi:10.1038/nsmb.2740

A 50-µl volume of this sample was applied on a Whatman 3MM filter. The filters were immediately washed with a solution of 10% trichloroacetic acid (TCA) and 0.5 µg/ml of methionine, boiled for 30 min and then washed three times with fresh cold TCA. Finally, the filters were rinsed with acetone and dried before radioactivity was determined with a scintillation counter. The incorporation of [methyl-^{3}H]T and [methyl-^{3}H]U was carried out with the protocol of Christensen-Dalsgaard and Gerdes[76]. After induction (time = 0), 1 ml of each culture was incubated at 37 °C with 50 µl of [methyl-^{3}H]T or [methyl-^{3}H]U. At each time point, 50 µl was put on a Whatman 3MM filter. The filters were immediately washed with a solution of 10% TCA and 0.5 µg/ml of dTTP or UTP, and then washed three times with fresh cold 10% TCA. Finally, the filters were rinsed with 95% ethanol and dried before radioactivity was determined with a scintillation counter.

Minimum purified *in vitro* translation assay with eTLC detection. All the components and proteins were prepared and purified exactly as described in the method of Fei *et al.*[37]. The [^{35}S]fMet-tRNA^{fMet} was prepared with the same protocol, but with the methionine replaced by 3 µM of [^{35}S]methionine (PerkinElmer) and quenched 5 min after the beginning of the reaction with 16 µM of cold methionine. Estimation of aminoacylation and formylation yields was assessed by hydrophobic interaction chromatography[37]. The Glu-tRNA^{Glu} was prepared as were the other aa-tRNAs[37]. The Glu-tRNA synthethase was prepared as described by Shimizu *et al.*[77]. All the minimum purified *in vitro* translation assays were done in Polymix buffer (50 mM Tris-OAc, pH 6.9, 100 mM KCL, 5 mM NH_4OAc, 0.5 mM $Ca(OAc)_2$, 0.1 mM EDTA, 1 mM spermidine, 5 mM putrescine, 3.5 mM $Mg(OAc)_2$, and 6 mM 2-mercaptoethanol) with 0.3 µM [^{35}S]fMet-tRNA^{fMet} with the pT7gp32.1–20 mRNA template (described in **Supplementary Note**).

The experiments presented in **Figure 4** and **Supplementary Figure 7** were performed with the standard procedure[37], which includes a GTP-regenerating system. Because it was not possible to use this protocol for experiments conducted with WT EttA at different concentrations of ATP and ADP, the GTP-regenerating system was omitted, and the GTP concentration was adjusted to a final concentration of 0.3 mM. For all the minimum purified *in vitro* translation assays, the reaction products were analyzed on eTLC after hydrolysis of the product with 0.2 M of KOH and separation of the products by eTLC with the method described by Youngman *et al.*[39] A 0.5-µl volume of each sample was spotted onto TLC-cellulose (EMD Chemicals) plates, dried and separated by electrophoresis in pyridine acetate buffer, pH 2.8 (20% glacial acetic acid and 0.06% f pyridine), at 1,200 V for 20 min.

Standard *in vitro* minimum purified translation assays with the GTP-regenerating system were performed at 37 °C with an mRNA pT7gp32.1–20 at 1.7 µM, [^{35}S]fMet-tRNA^{fMet} (0.3 µM), 70S ribosome (0.45 µM), the initiation factors (~0.5 µM each), the corresponding aa-tRNA (0.7 µM) and the elongation factors (EF-Tu 2 µM, EF-Ts 1 µM, and EF-G 1.5 µM). The reactions were performed in the presence or absence of WT EttA or EttA-EQ$_2$ (2.5 µM) with ATP (0.5 mM) at different steps of the reaction. The reaction was assembled in sequential order: first, the 70S IC was assembled by incubation of the 70S ribosome and initiation factors (Ifs) 1, 2 and 3 in Polymix buffer with GTP for 10 min at 37 °C. Second, the mRNA was added and the reaction was incubated for another 10 min at 37 °C. Third, [^{35}S]fMet-tRNA^{fMet} was added, and another 10 min of incubation at 37 °C took place. Finally, the 70S IC was kept on ice for at least 10 min before being used for the elongation reactions. The reactions were assembled as described in the **Figure 3** legend. EF-G and ternary complex were prepared with the GTP-regenerating buffer as described by Fei *et al.*[37].

Standard *in vitro* minimum purified translation assays without the GTP-regenerating system were run with an equivalent protocol but with the following changes: after the formation of the 70S IC, the reaction was buffer-exchanged in Polymix buffer without GTP with a Zeba spin column (Thermo Scientific). The resulting GTP-free 70S IC was divided into aliquots and stored at −80 °C. The reactions were run with this 70S IC with nearly the same conditions as before. However, the 70S ribosome concentration was 0.6 µM, while the GTP concentration was 0.3 mM. All the reactions were done at room temperature to slow down the process. The reactions were run in the presence or absence of combinations of ATP (1.2 mM) and ADP (0.6 mM). After addition of the 70S IC, either buffer (control) or WT EttA (EttA) (3.5 µM) was added in parallel with the elongation factors Phe-tRNA^{Phe} and Lys-tRNA^{Lys}.

***In vivo* fitness assays.** MG1655 and the corresponding Δ*ettA* stain were grown overnight separately in LB at 37 °C and 250 r.p.m. Ampicillin was added at 100 µg/ml for complementation experiments, which were conducted with cells containing the pBAD, pBAD-ettA, pBAD-His$_6$-ettA or pBAD-ettA-Δarm plasmid. Immunoblotting analysis with anti-EttA antibody (unpublished data, G.B. and J.F.H.) demonstrates a roughly physiological level of expression from the pBAD-ettA plasmid under the growth conditions used in these experiments (i.e., without supplementation with glucose to repress expression from the arabinose promoter controlling expression of EttA). The overnight cultures were mixed together in a ratio of 1:1 on the basis of OD_{600} and diluted 100-fold into fresh LB. At the indicated times (24, 72, or 144 h), these cultures were diluted 1,000-fold into fresh medium. This serial regrowth procedure was repeated for the number of times indicated in the figure. For the 144-h experiment, the growth was continued after the second restart for only 24 h. All of the regrowth experiments were performed in triplicate with independent inocula. For PCR analysis, a 100-µl aliquot of each culture was centrifuged at 6,000 r.p.m for 5 min and washed in 1 ml of phosphate-buffered saline (PBS) buffer, and the resulting pellets were stored at −20 °C. The pellets were resuspended in 200 µl of milliQ water, and 0.5 µl of the resulting solution was added to 30 µl of Gotaq PCR reaction mix (Promega) with primers designed to hybridize 400 pb upstream and downstream of the *ettA* gene. After 20 cycles of PCR amplification (95 °C for 30 s, 55 °C for 30 s and 72 °C for 2 min), the products were separated on a 1% TBE agarose gel that was stained with ethidium bromide. The gel was imaged on a UV transilluminator with a camera configured to avoid saturation. The PCR assay was calibrated by analysis immediately after mixture of samples containing varying ratios of WT and Δ*ettA* cells. The calibration procedure demonstrated that the assay detects *ettA* cells with somewhat higher sensitivity, meaning that it provides a conservative estimate of the degree of depletion of the *ettA* cells. The most important results from the PCR-based assays of coculture content were verified by plating on LB-agar cells from one 8 × 24-h restart experiment and with colony PCR to determine the genotype of ten of the resulting single colonies. This assay showed that that nine colonies contained WT cells, whereas only one contained Δ*ettA* cells.

Analytical gel-filtration and static light-scattering analyses. Protein samples were injected onto a Shodex 804 column (Showa Denko, Tokyo, Japan) running at 4 °C in 150 mM NaCl, 5% (v/v) glycerol, and 20 mM Tris-Cl, pH 7.2. The column effluent was monitored with static-light scattering (Dawn) and refractive index (Optilab) detectors from Wyatt Technologies.

Immunochemistry. Polyclonal rabbit antiserum was generated by Invitrogen's EvoQuest division with purified EttA as an antigen. After protein separation on a 10% SDS-PAGE gel, electrotransfer onto nitrocellulose and blocking with 5% blotting-grade nonfat dry milk (Bio-Rad), immunoblots were incubated with a 1:20,000 dilution of antiserum from a terminal bleed and developed with the ECL system (GE Biosciences) with horseradish peroxidase–conjugated goat anti-rabbit secondary antibodies (NA9340V, GE Biosciences) at a dilution of 1:5,000. The specificity of both antibodies was verified as follows: preimmune serum did not show any immunoreactivity at the molecular weight of EttA. The specificity of the EttA antiserum was verified with *ettA*::Tn5 knockout, which did not show any immunoreactivity at the molecular weight of EttA in blots of whole cells cultured in LB medium (**Supplementary Fig. 5c**); the isogenic control strain MG1655 showed EttA immunoreactivity similar to that observed from strain DH5α. The antibody was also affinity purified against EttA with the affinity purification of polyclonal antisera described by Levin[78]. The western blot presented in **Supplementary Figure 5c** was incubated with a 1:2,000 dilution of affinity-purified anti-EttA antibody, developed with a donkey anti-rabbit secondary-antibody conjugate to IRDye 680 (926-32223, Li-cor) at a dilution of 1:10,000 (the specificity of the antibody was verified as described above) and scanned on an Odyssey CLx scanner (Li-cor).

Polysome analyses. Polysomes were isolated from WT strain MG1655 with the freeze-thaw-lysozyme lysis method of Ron *et al.*[79] with 0.1 mg/ml chloramphenicol added to the growth medium 10 min before harvesting and to the cell-lysis buffers. They were separated on 10–40% (w/v) sucrose gradients in a buffer containing 10 mM Mg-OAc, 20 mM Tris-OAc, pH 7.6, and

NH_4OAc 100 mM. The gradients were spun in a SW40Ti rotor at 40,000 r.p.m. for 2 h before manual fractionation with a Brandel Model 184 fractionator. Fractions were analyzed with SDS-PAGE and subsequent immunoblotting with anti-EttA antiserum. In the control experiment, 0.2 mg/ml RNase A (Sigma-Aldrich) was added to the polysome preparation before loading on the gradient. Polysomes were isolated from the strains overexpressing EttA or EttA-EQ_2 with the same protocol, but the starting strains were MG1655 Δ*ettA* cells containing pBAD-ettA or pBAD-ettA-EQ_2 plasmids. After reaching an OD_{600} of 0.6, cells were induced with 0.1% (w/v) L-arabinose for 10, 20, 30, or 40 min. The sucrose density-gradient profile in **Figure 3c**, which shows complete depletion of polysomes in the pBAD-ettA-EQ_2 cells at the 30-min time point, is representative of the results of three independent replicate experiments.

61. Berlyn, M.B. & Letovsky, S. Genome-related datasets within the *E. coli* Genetic Stock Center database. *Nucleic Acids Res.* **20**, 6143–6151 (1992).
62. Miller, J.H. *Short Course in Bacterial Genetics: A Laboratory Manual and Handbook for Escherichia coli and Related Bacteria* (Cold Spring Harbor Laboratory Press, Plainview, New York, 1992).
63. Datsenko, K.A. & Wanner, B.L. One-step inactivation of chromosomal genes in *Escherichia coli* K-12 using PCR products. *Proc. Natl. Acad. Sci. USA* **97**, 6640–6645 (2000).
64. Baba, T. *et al.* Construction of *Escherichia coli* K-12 in-frame, single-gene knockout mutants: the Keio collection. *Mol. Syst. Biol.* **2**, 2006.0008 (2006).
65. Neidhardt, F.C. & Curtiss, R. *Escherichia coli and Salmonella: Cellular and Molecular Biology* (ASM Press, Washington, DC, 1996).
66. Otwinowski, Z. & Minor, W. Processing of X-ray diffraction data collected in oscillation mode. *Methods Enzymol.* **276**, 307–326 (1997).
67. Terwilliger, T.C. & Berendzen, J. Automated MAD and MIR structure solution. *Acta Crystallogr. D Biol. Crystallogr.* **55**, 849–861 (1999).
68. Terwilliger, T.C. Maximum-likelihood density modification using pattern recognition of structural motifs. *Acta Crystallogr. D Biol. Crystallogr.* **57**, 1755–1762 (2001).
69. Jones, T.A., Zou, J.-Y., Cowan, S.W. & Kjeldgaard, M. Improved methods for building protein models in electron density maps and the location of errors in these models. *Acta Crystallogr. A* **47**, 110–119 (1991).
70. Brünger, A.T. *et al.* Crystallography & NMR system: a new software suite for macromolecular structure determination. *Acta Crystallogr. D Biol. Crystallogr.* **54**, 905–921 (1998).
71. Adams, P.D. *et al.* PHENIX: a comprehensive Python-based system for macromolecular structure solution. *Acta Crystallogr. D Biol. Crystallogr.* **66**, 213–221 (2010).
72. Emsley, P., Lohkamp, B., Scott, W.G. & Cowtan, K. Features and development of Coot. *Acta Crystallogr. D Biol. Crystallogr.* **66**, 486–501 (2010).
73. Collaborative Computational Project, Number 4. The CCP4 suite: programs for protein crystallography. *Acta Crystallogr. D Biol. Crystallogr.* **50**, 760–763 (1994).
74. Kleywegt, G.J. Quality control and validation. *Methods Mol. Biol.* **364**, 255–272 (2007).
75. Hirashima, A. & Inouye, M. Specific biosynthesis of an envelope protein of *Escherichia coli*. *Nature* **242**, 405–407 (1973).
76. Christensen-Dalsgaard, M. & Gerdes, K. Two higBA loci in the *Vibrio cholerae* superintegron encode mRNA cleaving enzymes and can stabilize plasmids. *Mol. Microbiol.* **62**, 397–411 (2006).
77. Shimizu, Y. *et al.* Cell-free translation reconstituted with purified components. *Nat. Biotechnol.* **19**, 751–755 (2001).
78. Levin, P.A. in *Methods in Microbiology* Vol. 31 (ed. Philippe Sansonetti, A.Z.) 115–132 (Academic Press, 2002).
79. Ron, E.Z., Kohler, R.E. & Davis, B.D. Polysomes extracted from *Escherichia coli* by freeze-thaw-lysozyme lysis. *Science* **153**, 1119–1120 (1966).

doi:10.1038/nsmb.2740